31st Annual International Conference of the IEEE EMBS
Minneapolis, Minnesota, USA, September 2-6, 2009

Electrical Conductivity Imaging using MRI Measurement of the Magnetic Field Vector

Michael Joy *Member, IEEE*, Adrian Nachman, Tim DeMonte, Dinghui Wang, Weijing Ma

***Abstract*— Current density and electrical conductivity imaging research at the University of Toronto is reviewed. Methods for imaging live animals at low frequency are described and contrasted with EIT and other MRI based techniques. New work on imaging at radio frequencies is presented and future work directions are discussed. It is concluded that low frequency methods are mature and ready for application in small animals and that radio frequency methods will soon have application in small animals.**

I. Introduction

It has become increasingly clear that isotropic electrical conductivity can be measured accurately using magnetic resonance imaging (MRI) techniques and that this will permit better measurement of deep areas than electrical impedance tomographic (EIT) methods[2]. EIT, however, has its own significant advantages, such as its relative simplicity, availability and low cost. Nevertheless, the goal of using MRI to make these electrical measurements has attracted increasing attention.

Work toward this goal started at the University of Toronto in 1989 [3] with the discovery that an MRI could be used to measure applied electrical currents. The principle was to measure the magnetic field, $\mathbf{H}$, produced by the current and then take its curl

$$\nabla \times \mathbf{H} = \mathbf{J} \qquad (1)$$

to obtain the current density (CD), $\mathbf{J}$. The measurement of $\mathbf{H}$ was accomplished by applying DC current, $I(t)$, during a standard MRI imaging pulse sequence, in such a way as to accumulate phase in the complex MR image in regions where the applied current had caused a magnetic field. This phase would then equal the time integral of $\gamma\mu\mathbf{H}_Z$ where $\mathbf{H}_Z$ is the component of the field $\mathbf{H}$ parallel to the static MRI field, $\mathbf{B}_0$. Here γ is the gyromagnetic ratio and μ, the permeability constant. Since tissue is only weakly diamagnetic $\mu \approx \mu_0$. The waveform of $I(t)$ was initially chosen to be bipolar [4, 5] and was placed in a spin echo sequence to assure that the only phase in the image was due to $\mathbf{H}_Z$. To allow faster imaging we now use a fast gradient echo sequence and ±cycled unipolar current pulses [6]. We call these methods low frequency current density imaging (LFCDI). LFCDI as described in [4, 5] images both conductive and polarization currents, however the latter are usually small in tissues for the 1-10 ms current pulses we employ. It has been pointed out, however, that the sequence can be altered to separate mobile-ion current from immobile-ion current [7].

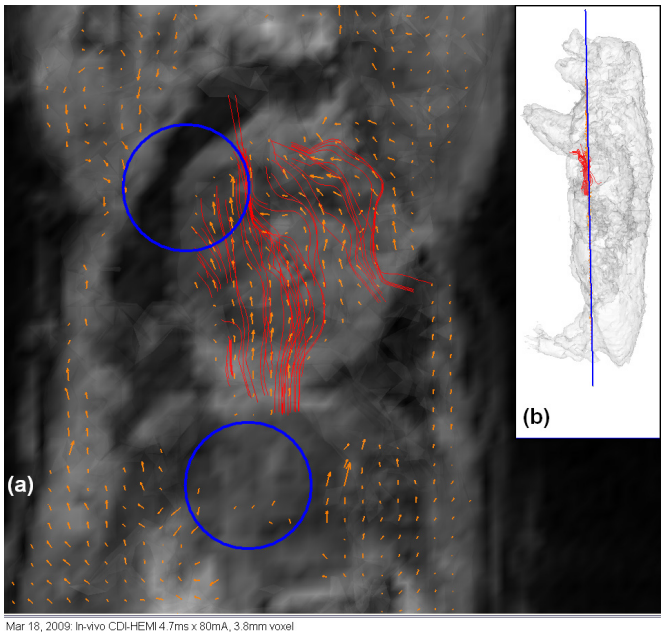

Fig. 1. Current density (CD) image of a live pig. Three dimensional (3D) data is projected onto a 2D plane, as indicated by a straight line in (b). CD data from one (of many) slices is shown as arrows projected into the plane. A selection of 3D CD streamlines is superimposed in (a) and (b). MRI magnitude in the plane is also shown in (a) and used in an iso-surface in (b). Circles show current electrode positions on skin. Note the complicated current paths between the electrodes.

To apply equation (1) we measure all three components of $\mathbf{H}$ by rotating the subject in the bore of the magnet. While this restricts the size of our subjects we find that we can complete a LFCDI image of a living subject in 30 minutes and can be assured of the accuracy of our results. Measuring current density is valuable in studies where current is applied externally (transcranial stimulation [8], cardiac defibrillation [9], muscular stimulation [10], Tasers and HEMI [6]).

While LFCDI is valuable, a method for accurately measuring tissue conductivity would be more generally applicable. Work with this goal started in Toronto in 1992 . Shortly after this it was suggested that conductivity images could be made using even a single component of $\mathbf{H}$ [11, 12] together with surface data. We found that it was possible to compute isotropic conductivity directly from two

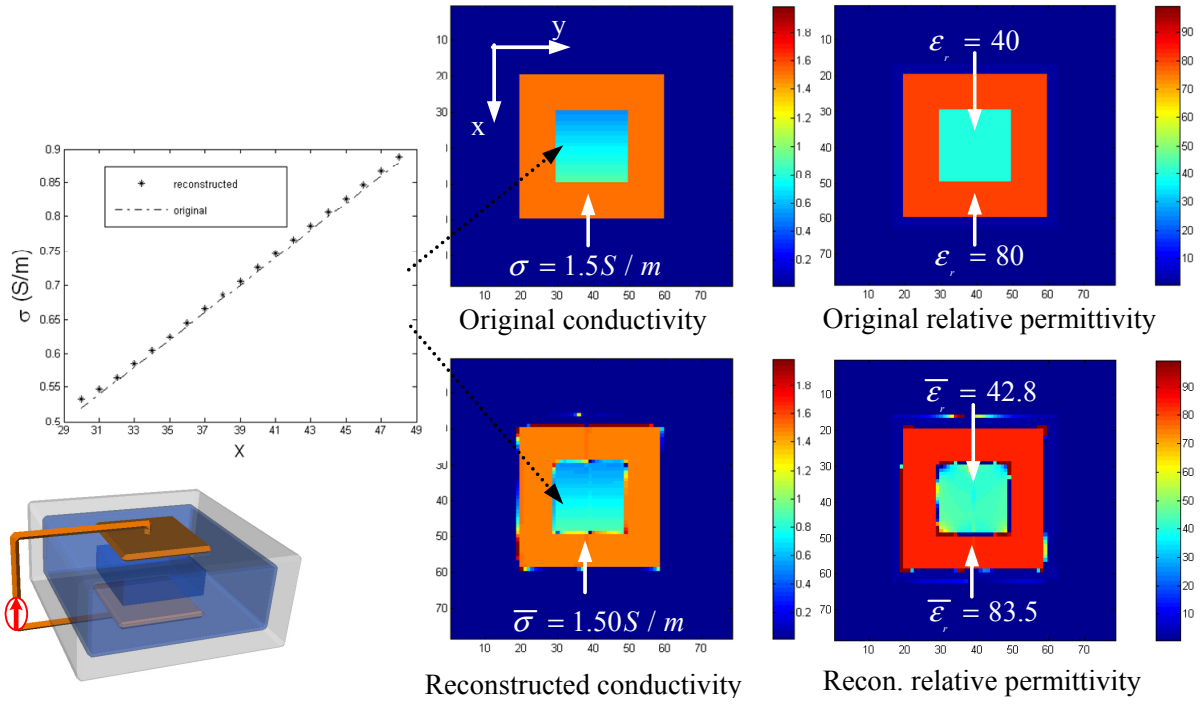

Fig. 2. Simulation of RFCDII. Equation 4 is used to compute inhomogeneous complex conductivity.

different current densities, $\mathbf{J}_1$ and $\mathbf{J}_2$, without measuring any surface potential [13] using the novel explicit formula :

$$\nabla \ln \sigma = \frac{(\nabla \times \mathbf{J}_2 \square \mathbf{M})\mathbf{J}_1 - (\nabla \times \mathbf{J}_1 \square \mathbf{M})\mathbf{J}_2 + (\nabla \times \mathbf{J}_1 \square \mathbf{J}_2)\mathbf{M}}{|\mathbf{M}|^2} \quad (2)$$

where $\mathbf{M} = \mathbf{J}_1 \times \mathbf{J}_2$. This was also independently shown by Lee [14]. We demonstrated this result in tissue [15] and later in a phantom [2] where its high accuracy could be confirmed. This result shows that local LFCDI measurements can reliably measure the conductivity differences between points. We call this Low Frequency Current Density Impedance Imaging (LFCDII).

Immediately after the development of LFCDI, a similar method, Radio frequency CDI (RFCDI), for imaging current at the Larmor frequency (e.g. 64 MHz at 1.5T) was devised and tested in Toronto [16]. RFCDI measured the two left circularly polarized (LCP) transverse components of the radio frequency (RF) magnetic field produced by an applied RF current. Clearly this measurement alone does not allow computation of current density using equation (1) since it requires all three components of $\mathbf{H}$ (i.e. both left and right circularly polarized components and the longitudinal component). Scott [17] showed, however, that the longitudinal component of the RF current density could be computed from these two measurements provided that this component was much larger than the partial derivative of the corresponding longitudinal magnetic field component. Scott also showed that the missing components of $\mathbf{H}$ could be acquired by rotating the subject in the bore of the magnet as with LFCDI [18]. The problem with this suggestion was that the applied currents might induce currents in the imager and these would not be rotated with the object.

Recently we have shown that, for a phantom in a clinical 1.5T imager, it is possible to perform a 180 degree rotation and obtain the complete transverse RF field [19]. This allows RFCDI of the longitudinal CD without the assumption used by Scott. We indicated that a third 90 degree rotation about the same axis may be performed with this phantom and the complete field $\mathbf{H}$ measured. We have also developed the original RFCDI technique by implementing [20] a multi slice version suggested by Scott [1] and by developing a method [21] that allows Scott's polar decomposition method [17] to allow phase wrapping and thus the potential capability to image higher CD than is possible with the present "rotary echo" method [17].

We have also addressed the goal of measuring the RF conductivity from RFCDI images (RFCDII). As a step towards this we have devised a formula [22] based on equation (1) and

$$\nabla \times \mathbf{E} = -\frac{\partial \mathbf{B}}{\partial t} \quad (3)$$

where $\mathbf{E}$ is the RF electric field induced by the RF magnetic field $\mathbf{B} = \mu_0 \mathbf{H}$ due to an applied RF current. The formula

$$\sigma + j\omega\varepsilon = -j\frac{(\nabla^2 \mathbf{H}) \cdot (\nabla \times \mathbf{H})}{\omega\mu_0 \mathbf{H} \cdot (\nabla \times \mathbf{H})} \quad (4)$$

has been tested on simulated data with inhomogeneous complex conductivity and works well provided that the term

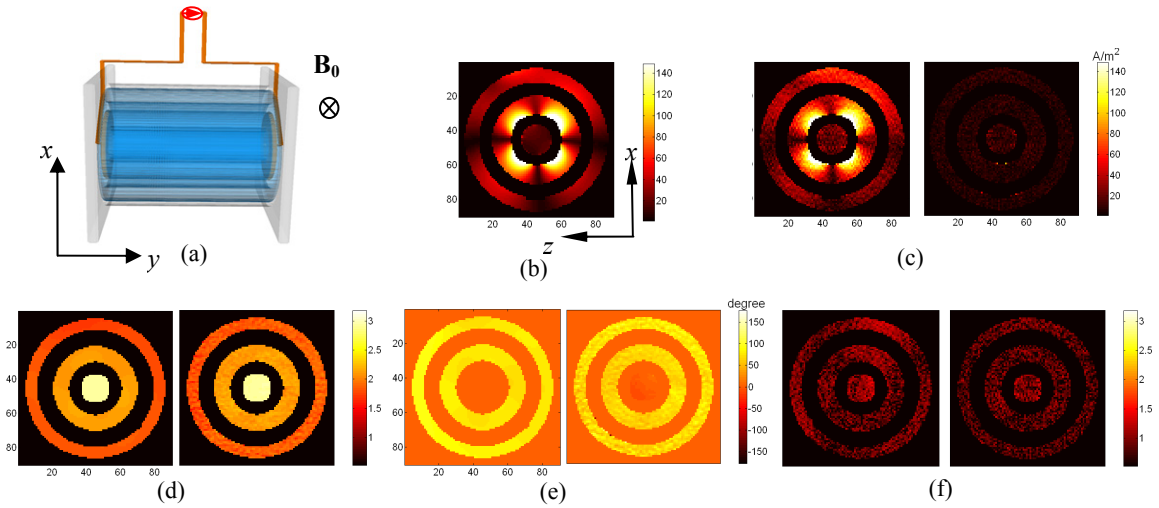

Figure 3: RF current density vector reconstruction based on 1 2 or 3 orientations.. (a) A three-chamber phantom filled with doped saline placed with its axis perpendicular to $\mathbf{B_0}$. The same ZX slice is shown in all images regardless of which component of the CD is being displayed. CD components are relative to the frame shown in (a).

$\mathbf{H}\cdot(\nabla\times\mathbf{H})$ in the denominator is not small. The results of this simulation are shown in Fig. 2.

This numerical FDTD simulation, of the object shown Fig. 2 bottom left, was done at 64MHz and was intended to demonstrate that equation (4) recovers a linearly varying complex conductivity. No noise was added to the $\mathbf{H}$ data. Differentiation was performed with a 2D 2x1 template. The graph shown is of the average conductivity along the y direction. in the indicated central region. Similar results were found at 300MHz for linearly varying permittivity and conductivity.

II. Current Work

We continue to work on the application of LFCDI to small animals (<5.3kg pigs). We are able to gather a complete LFCDI cardiac gated image of the whole live animal with 4mm cubical pixels in 30 minutes. Current pulses 1-4ms long with up to 110mA can be obtained. Over a 6 hour period, 10-12 such images can be obtained from the same animal. The Fig. 1 shows recent experimental data. In (a) CD vectors are shown in the coronal plane indicated in (b). The magnitude of the CD is proportional to the length of the arrow. We acquire such data over the whole animal. The circles in (a) indicate the positions of the electrodes. Streamlines in (a) are drawn in three dimensions using the CD data. We are building equipment to allow impedance imaging using equation (2) as well. Our goal here is to show how the LFCDI technique can be used in small animals to reliably measure current density and conductivity at a large number of points in a live subject.

Additionally we are endeavoring to apply RFCDI and RFCDII to small animals as well. We will use equation(4) for RFCDII ,and investigate a better local method that avoids the constraint on $\mathbf{H}\cdot(\nabla\times\mathbf{H})$. We will work at 1.5T initially to avoid the problems (see footnote) in measuring the complete magnetic field $\mathbf{H}$ at higher frequencies. The problem of measuring both circular polarities of $\mathbf{H}$ will be addressed by rotations as with LFCDI. An example of recent steps in this direction is shown in Fig. 3. A 90 and a 180 degree rotation are used to obtain for the first time both the right and left circularly polarized RF current induced magnetic field components in all three directions. The restrictive assumption used by Scott [17] is not required. The phantom, figure 3(a), has three, water filled, cylindrical chambers separated by solid walls. Only the inner region contains sodium chloride. The electrodes cover the inner two chambers. Since two electrodes are attached to both ends, current flows mainly in the axial (y) direction. Thus CD J_y is non zero while J_z and J_x should be very small in comparison to J_z Figure 3(b) is simulated data and displays the magnitude of the difference between the simulated CD, J_z (~0) , and the J_z computed from the (simulated) magnetic fields available in the position shown in (a) alone using Scott's assumption. Note that the erroneous large J_z arises because Scott's assumption is not justified in position (a). Figure 3(c) displays the difference between the simulated CD J_z and the measured magnetic fields available with no rotations (left) and with a 180 degree rotation (right). Note that the errors on the left are predicted by the simulation and that these errors disappear when the complete H_x H_y field is measured.

With an additional 90 rotation, J_x (~0) and J_y (finite) are recovered as well. Note that only rotations in the horizontal plane are required. All three orthogonal current density components are compared in Figure (d)-(f). Figure 3(d) and (e) compare the magnitude and phase of simulated and measured J_y. Figure 3(f) shows $|J_x|$(left) and $|J_z|$(right). Which are basically zero as expected. We conclude that we can measure for the first time the complete magnetic field produced by the RF current.

III. Conclusion

Our conclusion from this work is that LFCDI and LFCDII are mature and ready for application in small animals. RFCDI and RFCDII will soon have application in small animals. The issues anticipated at high fields will be addressed by migration to a 3T imager. The dependence on rotations is still an impediment to human application that we hope can be overcome. The rotations required for RF methods are about one axis and thus easier to accommodate. The problems at higher frequencies referred to above are associated with the increased interaction of the RF imaging fields with the dielectric object and were anticipated early by Scott [1]. They presently present an unsolved problem.

References

[1] G. C. Scott, "NMR Imaging of Current Density and Magnetic Fields," *Electrical Engineering*. PhD Toronto: University of Toronto, 1993, ProQuest AAT NN92914 p. 273.

[2] K. F. Hasanov, A. W. Ma, A. I. Nachman, and M. L. G. Joy, "Current density impedance imaging," *IEEE Transactions on Medical Imaging,* vol. 27, pp. 1301-1309, Sep 2008.

[3] M. L. G. Joy, G. C. Scott, and R. M. Henkelman, "In-Vivo Detection of Applied Electric Currents by Magnetic Resonance Imaging," *Magnetic Resonance Imaging,* vol. 7, pp. 89-94, 1989.

[4] G. C. Scott, M. L. G. Joy, R. L. Armstrong, and R. M. Henkelman, "MEASUREMENT OF NONUNIFORM CURRENT-DENSITY BY MAGNETIC-RESONANCE," *IEEETransactions on Medical Imaging,* vol. 10, pp. 362-374, Sep 1991.

[5] G. C. Scott, M. L. G. Joy, R. L. Armstrong, and R. M. Henkelman, "SENSITIVITY OF MAGNETIC-RESONANCE CURRENT-DENSITY IMAGING," *Journal of Magnetic Resonance,* vol. 97, pp. 235-254, Apr 1992.

[6] T. P. DeMonte, J. H. Gao, D. H. Wang, W. J. Ma, and M. L. G. Joy, "Measurement of Current Density Vectors in a Live Pig for the Study of Human Electro-muscular Incapacitation Devices," in *30th Annual International Conference of the IEEE-Engineering-in-Medicine-and-Biology-Society*, Vancouver, CANADA, 2008, pp. 5842-5845.

[7] I. Sersa, "Current density imaging sequences with separation of mobile-ion current from immobile-ion current," *Journal of Magnetic Resonance,* vol. 196, pp. 33-38, Jan 2009.

[8] M. L. G. Joy, V. P. Lebedev, and J. S. Gati, "Imaging of current density and current pathways in rabbit brain during transcranial electrostimulation," *IEEE Transactions on Biomedical Engineering,* vol. 46, pp. 1139-1149, Sep 1999.

[9] R. S. Yoon, T. P. DeMonte, K. F. Hasanov, D. B. Jorgenson, and M. L. G. Joy, "Measurement of thoracic current flow in pigs for the study of defibrillation and cardioversion," *IEEE Transactions on Biomedical Engineering,* vol. 50, pp. 1167-1173, OCT 2003.

[10] A. Patriciu, K. Yoshida, J. J. Struijk, T. P. DeMonte, M. L. G. Joy, and H. Stodkilde-Jorgensen, "Current density imaging and electrically induced skin burns under surface electrodes," *IEEE Transactions on Biomedical Engineering,* vol. 52, pp. 2024-2031, Dec 2005.

[11] E. J. Woo, S. Y. Lee, and C. W. Mun, "Impedance tomography using internal current density distribution measured by nuclear magnetic resonance," *Proceedings of SPIE,* vol. 2299, pp. 377-385, 1994.

[12] E. J. Woo and J. K. Seo, "Magnetic resonance electrical impedance tomography (MREIT) for high-resolution conductivity imaging," *Physiological Measurement,* vol. 29, pp. R1-R26, Oct 2008.

[13] K. F. Hasanov, A. W. Ma, R. S. Yoon, A. I. Nachman, and M. L. Joy, "A new approach to Current Density Impedance Imaging (CDII)," in *ISMRM Annual Meetiing*, Kyoto, Japan, 2004, p. 2356.

[14] J. Y. Lee, "A reconstruction formula and uniqueness of conductivity in MREIT using two internal current distributions," *Inverse Problems,* vol. 20, pp. 847-858, Jun 2004.

[15] W. Ma, D. Wang, T. DeMonte, A. Nachman, D. Jorgenson, and M. Joy, "Current Density Impedance Imaging in Porcine Heart," in *ISMRM 14th Scientific Meeting & Exhibition*, Seattle, 2006, p. 3379.

[16] G. C. Scott, M. L. G. Joy, R. L. Armstrong, and R. M. Henkelman, "RF CURRENT-DENSITY IMAGING IN HOMOGENEOUS MEDIA," *Magnetic Resonance in Medicine,* vol. 28, pp. 186-201, Dec 1992.

[17] G. C. Scott, M. L. G. Joy, R. L. Armstrong, and R. M. Henkelman, "ROTATING-FRAME RF CURRENT-DENSITY IMAGING," *Magnetic Resonance in Medicine,* vol. 33, pp. 355-369, Mar 1995.

[18] G. C. Scott, M. L. G. Joy, R. L. Armstrong, and R. M. Henkelman, "ELECTROMAGNETIC CONSIDERATIONS FOR RF CURRENT-DENSITY IMAGING,"*IEEE Transactions on Medical Imaging,* vol. 14, pp. 515-524, Sep 1995.

[19] D. Wang, W. Ma, T. P. DeMonte, A. I. Nachman, and M. L. Joy, "Experimental Testing of Radio Frequency Current Density Imaging with a Single 180-degree Rotation," in *ISMRM 16th Scientific Meeting & Exhibition*, Toronto, 2008, p. 1527.

[20] D. Wang, T. P. DeMonte, W. Ma, M. L. Joy, and A. I. Nachman, "Multi-slice Radio Frequency Current Density Imaging," *IEEE Transactions on Medical Imaging,* 2009.

[21] W. Ma, "Polar Decomposition Radio-Frequency Current Density Imaging with Dual-Unwrapping: Simulation and Experimental Results," in *ISMRM 16th Scientific Meeting & Exhibition*, Toronto, 2008, p. 1526.

[22] A. Nachman, D. Wang, W. Ma, and M. Joy, "A Local Formula for Inhomogeneous Complex Conductivity as a Function of the RF Magnetic Field," in *ISMRM 15th Scientific Meeting & Exhibition* Berlin: ISMRM http://www.ismrm.org/07/Unsolved.htm, 2007.